50 Grades of Shade

ARIANE MIDDEL*
School of Arts, Media and Engineering (AME)
School of Computing, Informatics, and Decision Systems Engineering (CIDSE)
Arizona State University
950 S. Forest Mall, Stauffer B, Tempe, AZ 85281
ariane.middel@asu.edu

SAUD ALKHALED
College of Architecture
Kuwait University
saud.alkhaled@ku.edu.kw

FLORIAN A. SCHNEIDER
School of Sustainability
Arizona State University
florian.schneider@asu.edu

BJOERN HAGEN
School of Sustainability
Arizona State University
bjoern.hagen@asu.edu

PAUL COSEO
The Design School
Arizona State University
paul.coseo@asu.edu

*Correspondence concerning this article should be addressed to Ariane Middel, School of Arts, Media and Engineering, School of Computing, Informatics, and Decision Systems Engineering, Arizona State University, 950 S. Forest Mall, Stauffer B, Tempe, AZ 85281; telephone: +1 480-414-6793; e-mail: ariane.middel@asu.edu.

Early Online Release: This preliminary version has been accepted for publication in *Bulletin of the American Meteorological Society*, may be fully cited, and has been assigned DOI 10.1175/BAMS-D-20-0193.1. The final typeset copyedited article will replace the EOR at the above DOI when it is published.

Abstract: Cities increasingly recognize the importance of shade to reduce heat stress and adopt urban forestry plans with ambitious canopy goals. Yet, the implementation of tree and shade plans often faces maintenance, water use, and infrastructure challenges. Understanding the performance of natural and non-natural shade is critical to support active shade management in the built environment. We conducted hourly transects in Tempe, Arizona with the mobile human-biometeorological station *MaRTy* on hot summer days to quantify the efficacy of various shade types. We sampled sun-exposed reference locations and shade types grouped by urban form, lightweight/engineered shade, and tree species over multiple ground surfaces. We investigated shade performance during the day, at peak incoming solar, peak air temperature, and after sunset using three thermal metrics: the difference between a shaded and sun-exposed location in air temperature (ΔT_a), surface temperature (ΔT_s), and mean radiant temperature (ΔT_{MRT}). ΔT_a did not vary significantly between shade groups, but ΔT_{MRT} spanned a 50°C range across observations. At daytime, shade from urban form most effectively reduced T_s and T_{MRT}, followed by trees and lightweight structures. Shade from urban form performed differently with changing orientation. Tree shade performance varied widely; native and palm trees were least effective, while non-native trees were most effective. All shade types exhibited heat retention (positive ΔT_{MRT}) after sunset. Based on the observations, we developed characteristic shade performance curves that will inform the City of Tempe's design guidelines towards using "the right shade in the right place" and form the basis for the development of microclimate zones (MCSz).

Capsule Summary (30 words max): Human-biometeorological observations show that shade from urban form and engineered structures effectively reduces daytime thermal exposure and can be a viable alternative to trees in areas with infrastructure challenges.

Accepted for publication in *Bulletin of the American Meteorological Society.* DOI 10.1175/BAMS-D-20-0193.1.

1. Introduction

The year 2020 tied 2016 for the hottest year on record globally with the hottest meteorological summer in the northern hemisphere. Heat waves are expected to become more intense, occur more frequently, and last longer due to climatic changes (Meehl and Tebaldi 2004). In addition, urbanization alters the thermal characteristics of an area locally, contributing to urban heat and further challenging human health and well-being. Cities worldwide are concerned about health impacts of extreme heat exposure and now strategically plan for heatwaves as a way to decrease the risk of heat-related illness and mortality, especially in vulnerable populations. In this context, urban greening has emerged as an investment priority for municipalities to combat adverse effects of climate change and improve urban sustainability, human health, and quality of life (Norton et al. 2015). Trees cool the urban ecosystem through evapotranspiration and yield substantial thermal comfort benefits by providing shade (Bowler et al. 2010; Armson et al. 2013; Middel et al. 2016). Past studies have shown that trees significantly impact the radiative heat exchange between the human body and the environment by attenuating the amount of direct solar radiation that increases the body's heat load and UV exposure (Aminipouri et al. 2019; Downs et al. 2019; Kántor et al. 2016; Parisi et al. 2019). Shade also lowers the radiative load on the body by reducing reflected and emitted heat from ground surfaces (Lindberg and Grimmond 2011; Middel and Krayenhoff 2019; Speak et al. 2020).

Capitalizing on the demonstrated cooling impacts of green infrastructure and the numerous economic, environmental, and social co-benefits of trees (Gregory McPherson 1992; Salmond et al. 2016, Klemm et al. 2015), cities around the globe—from Austin, Texas, USA (The City of Austin 2013) to Sydney, Australia (City of Sydney 2013)—have adopted urban forestry plans with ambitious canopy goals as a framework to invest in tree planting and

minimize heat risks. Yet, the implementation of those plans often conflicts with grey infrastructure provision in a mosaic of private and public property (Langenheim et al. 2020; Pataki et al. 2011; Roman et al. 2020). Engineered systems such as underground water utilities, communication cables, and overhead power lines stand in direct competition for limited space in the city's rights-of-way. In desert cities, drought conditions and increased irrigation demands further create a cooling - water use tradeoff that raises water conservation concerns (Middel et al. 2012).

Trees are a nature-based solution for shading, but human thermal exposure can also be improved through engineered shade, such as umbrellas and shade sails (Colter et al. 2019; Garcia-Nevado et al. 2020; Shashua-Bar et al. 2011), and urban form including overhangs, and urban canyons (Crewe et al. 2016; Middel et al. 2014; Lee et al. 2018; Pearlmutter et al. 1999; Johansson and Emmanuel 2006). To date, little is known about the cooling impact of these shading strategies, and cities lack actionable information for integrated green and grey infrastructure planning that incorporates viable shade alternatives into active shade management practices.

This study aims to quantify the efficacy of various shade types in hot, dry Tempe, Arizona, U.S.A. where human thermal exposure is mainly driven by incoming solar radiation. We assess shade performance using biometeorological observations of three human-relevant temperature measures: air temperature (T_a), surface temperature (T_s), and mean radiant temperature (T_{MRT}, see section 2.3). Based on observed T_{MRT} reductions, we develop typical shade performance curves that can help cities implement the "right shade in the right place" depending on urban context and function of space.

2. Methods

2.1 Study Area

The City of Tempe (33°25′28.6″N, 111°56′18.6″W) is a municipality in the Phoenix metropolitan area, Arizona in the Southwestern U.S.A. (Figure 1). The city covers an area of 104 km^2 and is home to 192,000 residents (U.S. Census, 2018). Situated in the heart of the Sonoran Desert, Tempe has a subtropical desert climate (Köppen Climate Classification subtype *Bwh*). Summers are hot and dry with an average of 175 days that have a temperature maximum at or above 32°C (90°F) and 110 days at or above a temperature maximum of 38°C (100°F) (NOAA, 2020). Mean minimum temperature is above 20°C between July and September (Western Regional Climate Center, 2020). On average, Tempe receives 237 mm of annual precipitation with peak rainfall occurring during the monsoon season running from mid-June through September. Tempe has about 300 clear days per year and averages 4,041 hours of sunshine of a possible 4,383 (92.2%).

The City is encouraging more compact real estate developments in Downtown Tempe with shade-producing mixed-use high-rise residential and commercial buildings. Outside the city center, Tempe is characterized by lower density development patterns with detached single-family homes (open low-rise Local Climate Zone) in gridded subdivisions. In 2017, the City adopted an Urban Forestry Master Plan (City of Tempe 2017) to increase tree and shade canopy from a city-wide average of 13 up to 25% by 2040 with focus on parks, streets, and urban hubs (i.e., compact shopping, entertainment, and civic areas). Almost all urban trees require irrigation due to the desert conditions.

[**Figure 1**]

We focused our shade investigations on two areas: Downtown Tempe (Figure 1A) and Kiwanis Park (Figure 1B). The Mill Avenue District in downtown is a shopping and entertainment

area that mainly provides shade through urban form and street trees. The Arizona State University Tempe Campus in downtown features various lightweight and engineered shade types (e.g., umbrellas, shade sails, solar structures) and shade trees. Kiwanis Park is a 125 acre City park with a lake, various sports fields, picnic areas, playgrounds, a recreation center, and multi-use paths. Shade in the park is predominantly provided by trees, gazebos, and a large shade sail covering a playground.

2.2 Data Collection

We conducted nine field trips between 2016 and 2019 on clear, hot summer days to collect shade performance data for 159 unique locations in Downtown Tempe (July 12 & 16, 2016; August 7, 2016; June 7-9, 2018; July 3 & 8, 2019) and Kiwanis Park (July 15, 2019). Each day, we performed microclimate transects at walking speed using the human-biometeorological instrument platform *MaRTy* (Middel and Krayenhoff 2019; Middel et al. 2020) (Figure 2, Table 1). *MaRTy* observes georeferenced, pedestrian-height 6-directional longwave (L_i) and shortwave (K_i) radiation flux densities, T_a, T_s (from up-welling longwave radiation), horizontal wind speed (v), and relative humidity (RH) at 2 s intervals. In 2016 and 2018, transects were conducted hourly between 8:00 Local Standard Time (LST) and 21:00 LST. Additional transects were conducted in 2019 during peak incoming K (12:00–13:00 LST), close to peak T_a (15:00–16:00 LST), and after sunset (20:00–21:00 LST). Each transect route took 50–60 mins to complete and included a 45–60 s stop at 20–30 locations of interest to account for the response time of the T_a/RH probe (22 s) and minimize the impact of sensor lag (Häb et al. 2015). The character of the shade did not change substantially during the 45–60 s stop. At each location, the up/down facing net radiometer was positioned in the center of the shade type. The cart was positioned such that it would not shade the observed surface under the net radiometer.

Accepted for publication in *Bulletin of the American Meteorological Society*. DOI 10.1175/BAMS-D-20-0193.1.

[**Figure 2**]

We selected a wide range of shade types that cover diverse ground surfaces (concrete, asphalt, gravel, grass) and grouped them into three categories: 1) lightweight or engineered shade, 2) shade from urban form, and 3) natural shade from trees (Figure 3). Lightweight or engineered shade includes non-permanent structures such as umbrellas and shade sails, pergolas, and engineered canopies (e.g., roofs and photovoltaic structures). Shade from urban form consists of building-integrated shade (e.g., overhangs, arcades, tunnels, breezeways, and shade from street canyon geometry). Lastly, natural shade encompasses various native and desert-adapted trees that are common in Tempe. In addition, several sun-exposed locations with high sky view factors were selected along the transects to serve as reference locations.

[**Figure 3**]

2.3 Data Processing

MaRTy-observed 6-directional radiation flux densities were summarized as T_{MRT} using angular factors W_i for a standing reference person (0.06 for the up/down facing sensors, 0.22 for lateral sensors) and absorption coefficients for shortwave ($a_k = 0.70$) and longwave ($a_l = 0.97$) radiation (Höppe 1992; VDI 1998; Kántor and Unger 2011): $T_{MRT} = \sqrt[4]{\frac{\sum_{i=1}^{6} W_i(a_k K_i + a_l L_i)}{a_l \cdot \sigma}} - 273.15\ K$ [°C]. Transect observations were extracted for each stop, and records affected by sensor lag were removed. For cross-site comparison, T_a and T_{MRT} observations were time-detrended to the middle of the transect hour using a linear correction factor (slope of temperature change during the transect). Since meteorological conditions were similarly hot between fieldwork days but not identical, we calculated thermal deltas between sun-exposed reference locations and shaded sites for the time-detrended transect stops. Shade performance was then assessed using three thermal metrics: the difference between shaded and sun-exposed reference site in air temperature ($T_{a,shade}$

– $T_{a,sun} = \Delta T_a$), surface temperature ($T_{s,shade} - T_{s,sun} = \Delta T_s$), and mean radiant temperature ($T_{MRT,shade} - T_{MRT,sun} = \Delta T_{MRT}$).

3. Results

Over the course of three summers and nine field work days, we collected 1,988 valid samples at 159 unique locations (Figure 1). A metadata table is provided in the electronic supplemental materials (Table A.1) and includes hemispherical photos, shade type, tree species, ground surface cover, albedo for sun-exposed locations, sky view factor (calculated from fisheye photos), and fractions of surrounding trees, buildings, impervious and pervious surfaces, and sky. The fractions were calculated from panoramic images using an image segmentation algorithm developed by Middel et al. (2019) using fully convolutional neural networks. Meteorological conditions on all field work days were similarly hot, dry, and sunny (Table A.2). The maximum daily T_a at Sky Harbor airport (7–11 km north-west of the study sites) ranged from 39.4–44.4°C with a minimum daily *RH* of 3.2–18.3% and a maximum daily *RH* of 19.0–48.9%. Wind speeds were low and ranged from 2.2–4.0 m s^{-1}. Incoming solar radiation peaked between 919 W m^{-2} and 983 W m^{-2}. On average, the study sites exhibited lower T_a than the airport at peak *K* (up to 1.6°C), peak T_a (up to 1.5°C), and especially after sunset (up to 4.6°C).

We conducted an independent samples t-test for the three observed thermal metrics to investigate if the differences in hourly T_a, T_s, and T_{MRT} between shade and sun are statistically significant (Table A.3). Test results for T_{MRT} and T_s were highly statistically significant ($p<0.001$) between 8:30 LST and 18:30 LST and after sunset. During the transition periods in the morning (7:30–8:30 LST) and evening (18:30–19:30 LST), the difference in T_{MRT} and T_s between shade and sun was less significant ($p<0.05$) or not significant. T_a did not vary much between shaded and unshaded locations. T_a t-test results were highly significant from 9:30–10:30 LST and 16:30

Accepted for publication in *Bulletin of the American Meteorological Society.* DOI 10.1175/BAMS-D-20-0193.1.

–17:30 LST, but average T_a differences were smaller than 1.3°C (Figures A.1 and A.2). An ANOVA for observed hourly thermal metrics between shade groups yielded similar results. T_{MRT} and T_s varied significantly ($p<0.001$) between shade groups from 9:30–17:30 LST and after sunset, while T_a differences were small and mostly not significant. Subsequently, we focus the shade performance assessment on ΔT_s and ΔT_{MRT} considering the cooling benefit of shade by group (urban form, lightweight/engineered, natural), type (e.g., shade sail, umbrella, awning, tree species), over different ground surfaces (impervious, gravel, grass/soil), and at various times of day: hourly average at daytime (after sunrise and before sunset), peak incoming K at 12:30 LST, close to peak T_a at 15:30 LST, and after sunset at 20:30 LST.

3.1 Shade Performance: Surface Temperature Cooling

Unshaded impervious surfaces reached a T_s of up to 64.5°C in the afternoon of June 9, 2018 when T_a was 41.0 °C. The same day, gravel T_s peaked at 61.2°C. T_s of grass did not exceed T_a throughout the day. We note that the grass surfaces observed in this study were fully irrigated using automated sprinkler systems. All shade types significantly reduced T_s, but the cooling magnitude varied by ground surface, shade group, and shade type. Urban form was most effective in cooling impervious surfaces followed by trees and lightweight structures (Figure 4). ΔT_s for impervious surfaces was -18.2 °C at 12:30 LST and -17.8°C at 15:30 LST, bringing T_s close to T_a. In general, T_s reduction from shade peaked between 12:30–15:30 LST for all surface types and shade groups (Figure A.3 and A.4). While shaded impervious surfaces stayed 2.7–4.5°C cooler after sunset than sun-exposed reference surfaces, gravel and grass exhibited a positive ΔT_s of 0.5°C and 1.6°C, respectively.

[**Figure 4**]

Trees over gravel achieved the best T_s cooling for any surface type with ΔT_s = -21.2°C at 12:30 LST and ΔT_s = -19.6°C at 15:30 LST. For all other surface types, trees displayed an average cooling magnitude of ΔT_s = -13.5°C at 12:30 LST, ΔT_s = -13.0°C at 15:30 LST, and ΔT_s = -2.9°C at 20:30 LST (Figures A.5–A.8), but results varied widely by tree species. Non-native evergreen trees such as the Canary Island Pine (*Pinus canariensis*), Indian Laurel (*Ficus Nitida*), and non-native deciduous trees such as the North Indian Rosewood (*Dalbergia sissoo*) exceeded 13°C in average impervious surface cooling during the day. Native trees such as Honey Mesquite (*Prosopis glandulosa*) and Palo Verde (*Parkinsonia sp.*) reduced T_s by 8.8°C, and palm trees (*Phoenix Sp.*) were least effective with an average ΔT_s of -5.6°C.

In the "urban form" shade group, the breezeway performed best at surface cooling with a daytime average ΔT_s of -23.4°C, closely followed by the tunnel, overhang, and arcade with a 15–16°C reduction in T_s. Most of the lightweight and engineered structures were slightly less effective at T_s cooling than trees with a cooling magnitude of 11–14°C between 12:30 LST and 15:30 LST. PVC and cloth umbrellas provided the least amount of T_s reduction with an average cooling magnitude of 6.9°C.

3.2 Shade Performance: Mean Radiant Temperature Reduction

The hottest T_{MRT} was observed at 16:30 LST on July 12, 2016 at a sun-exposed reference site with impervious ground cover (76.2°C), and the coolest T_{MRT} was recorded after sunset on June 19, 2018 over grass (24.7°C). The histogram of all observed ΔT_{MRT} values across dates and times exhibited a bimodal distribution (Figure 5). Binning ΔT_{MRT} into 1°C intervals yielded 50 bins from a minimum ΔT_{MRT} of -39.6°C (best shade performance) to a maximum ΔT_{MRT} of 8.6°C (warming effect). In contrast, ΔT_s spanned 36 bins (from -25.3–9.6°C) and ΔT_a only 6 bins (from -3.8–2.0°C) (Figure A.). Values surrounding the local ΔT_{MRT} maximum at 1°C mostly included

sun-exposed locations and samples recorded after sunset when a slight heat retention was present at formerly shaded areas, similar to the surface warming effect observed for ΔT_s. The other peak mainly consisted of mid-day and afternoon observations with sites shaded by a tunnel, arcade, or overhang located at the left tail of the distribution (best shade performance).

[**Figure 5**]

All shade types significantly reduced T_{MRT} at daytime, but the cooling performance varied by shade group and type. The hourly progression of ΔT_{MRT} by shade group (Figure 6) followed a similar pattern as ΔT_s (Figure A.3) with three key differences: 1) cooling magnitudes for ΔT_{MRT} were generally larger than for ΔT_s; 2) ΔT_{MRT} displayed an immediate cooling benefit in excess of 17°C after sunrise due to the attenuation of shortwave radiation—a major contributor to T_{MRT}—while surfaces in the urban environment required time to absorb heat and warm up causing a lagged response in ΔT_s; and 3) The ΔT_{MRT} curve exhibited a dent around solar noon, which can be attributed to the weighting of the directional radiant flux densities. We calculated T_{MRT} for a standing person, i.e., observations from the upwards and downwards facing radiometers were weighted 6%, while the lateral observations were weighted 22%. Due to the dent in the curve, shade performance in the afternoon was slightly better than at peak solar.

Shade groups displayed a consistent performance ranking during the day; urban form reduced T_{MRT} most effectively followed by trees and lightweight structures (Figure 7). At the hottest time of day, lightweight structures were as effective as trees in reducing the heat load on the human body but were not as performant at midday and overall.

[**Figure 6**]

Similar to ΔT_s, ΔT_{MRT} was positive after sunset, which indicates warming and is caused by trapping of longwave radiation under the shade as compared to the exposed open site. Heat

206 retention was larger under shade from urban form and lightweight/engineered structures than
207 under trees. Average daytime ΔT_{MRT} by tree species (Figure A.10–A.14) ranged from a cooling
208 benefit of -16.7°C (*Prosopis glandulosa*) to -25.9°C (*Pinus canaiensis*). Non-native evergreens
209 performed better than native species due to higher leaf area density. Shade from urban form
210 reduced T_{MRT} by 22.8–30.9°C during the day except for the east-west canyon (just short of
211 20.0°C). The tunnel and breezeway consistently outperformed all shade types during the day but
212 also exhibited the largest longwave trapping at night with ΔT_{MRT} = 3.2°C. Umbrellas and shade
213 sails ranked lowest on the performance scale but still provided substantial daytime cooling of -
214 17.3°C ΔT_{MRT}.

215 [**Figure 7**]

216 *3.3 Characteristic Shade Performance Curves by Shade Type*

217 Based on our hourly human-biometeorological observations we developed characteristic shade
218 performance curves (diurnal ΔT_{MRT} progression) for all major shade types under investigation
219 (Figure 8). The empirically based graphs display the evolution of ΔT_{MRT} assuming a latitude of
220 33° and a sun path for mid-July. Each performance curve is an idealized example of a single
221 shade type's cooling impact isolated from its urban context (i.e., other surrounding features that
222 could potentially cast shadows) and over the same ground cover (impervious). The real-world
223 hemispherical images next to each graph are guiding examples to illustrate the shade types but
224 do not necessarily produce the same performance curve because of the surrounding urban
225 context. All curves represent the difference between shaded and sun-exposed reference T_{MRT} for a
226 person standing in the center of the shade (for horizontal shade, e.g., trees, lightweight structures,
227 building features) or in the center of the urban form arrangement providing the shade (vertical
228 structures, e.g., urban canyons and courtyards).

Figure 8 displays 12 graphs grouped by shade orientation: a) east/west, b) north/south, and c) orientation-independent cases (canopies, courtyards). Each graph includes two reference lines that are identical across diagrams and illustrate two shade performance extremes: 1) the solid horizontal yellow line represents a sun-exposed location for which $\Delta T_{MRT} = 0$ all day; 2) the solid black line represents a long tunnel in which the standing person does not receive direct shortwave radiation all day. The blue and grey dashed lines with intersecting arrows illustrate ΔT_{MRT} for average-sized shade types; the arrows indicate in which direction the curve shifts if the shade (or built view factor) was smaller or larger. The blue and red dashed lines with arrows in between show two extreme cases of a shade type, e.g., an urban canyon with high and low aspect ratio. Lastly, the brown and green dashed lines represent the shade performance of high canopy, low leaf area density (LAD) trees (small tree view factor) and low canopy, high LAD trees (large tree view factor).

[**Figure 8**]

Orientation does not impact shade performance of tunnels and breezeways because of the elongated design of the built form that prevents direct shortwave radiation from penetrating the space. Breezeways are slightly less effective than tunnels since they allow for more reflected and diffuse radiation. Orientation becomes important for smaller non-square horizontal structures such as bus stop shelters. An east-west orientation is favorable because shade provision is extended from peak solar into the late morning and early afternoon. Shade performance of overhangs also depends on orientation. While north reaching overhangs are almost as effective in reducing T_{MRT} as tunnels, west and east facing overhangs either perform well in the morning (west) or afternoon (east). Performance curves of shade sails, umbrellas, and other engineered canopies are comparable to bus shelters. Umbrellas are slightly less effective, because the fabric

radiates heat close to a person's head, but still provide substantial T_{MRT} reduction during most hours of the day. Least effective are palm trees with a brief, very localized T_{MRT} reduction. In general, tree shade performance varies widely between the palm tree case and trees with a high LAD and wide canopy. Courtyards and north south oriented urban canyons exhibit shade performance curves that are reverse of canopies: they provide shade in the morning and afternoon but not during midday. East west oriented urban canyons are most complex, and the shape of the curve highly depends on the aspect ratio and sun elevation angle.

4. Discussion

All shade types had a daytime cooling impact on the three thermal metrics, but the magnitude of this effect varied widely. ΔT_a differences by shade type and group were minor (< 1.3°C on average) and, for most hours of the day, not highly statistically significant. Previous studies have reported small shade impacts on T_a, but cooling is often less than 2.0°C. Cheung and Jim (2018) observed a mean daytime cooling effect of 0.6°C under trees in Hong Kong, and de Abreu-Harbich et al. (2015) found minor T_a differences between sun-exposed and tree-shaded locations in tropical Campinas, Brazil, with the strongest cooling of 0.9–2.8°C during midday. Studies in Manchester, UK and Szeged, Hungary could not detect an effect of single trees on T_a (Armson et al. 2013; Kántor et al. 2016). With respect to urban form and lightweight/engineered shade, Middel and Krayenhoff (2019) reported average T_a variations of less than 1.5°C during record breaking heat in Tempe, Arizona for locations shaded by a north-south canyon, tunnel, and photovoltaic canopy.

In contrast, all shade groups and types had a significant impact on ΔT_s throughout the day. The average cooling impact exceeded 10°C between 12:30 LST and 15:30 LST. Our ΔT_s results are comparable to a study in Bolzano, Italy that found an average T_s cooling of 19°C across three surface types (grass, asphalt, porphyry) during peak T_a (Speak et al. 2020).

Specifically, tree shade cooled underlying asphalt by 16.4°C, rock by 12.9°C, and grass by 8.5°C. Golden et al. (2007) investigated the thermal impacts of photovoltaic (PV) canopies and trees on pavement T_s and 2 m T_a in Phoenix, Arizona. They concluded that shade from PV structures provides greater thermal benefits diurnally than tree shade while also supporting peak energy demand and conserving water. Garcia-Nevado et al. (2020) took thermal images of textile shade sails spanning urban canyons in Cordoba, Spain and found that T_s in the shade was up to 16°C lower than in the sun. They highlight the importance of urban canyon orientation for shade performance; shade sails increased thermal comfort in north south streets and decreased energy use in east west streets. The study also reported a 2°C nighttime warming of ground surfaces due to heat trapping.

Our human-biometeorological observations are in line with previous studies that found shade to be the major driver of T_{MRT} in hot dry environments (Emmanuel et al. 2007; Ali-Toudert and Mayer 2007). Shade performance measured in ΔT_{MRT} was stronger than ΔT_s and ΔT_a with maximum T_{MRT} reductions close to 40.0°C. Results confirm the shade performance ranking Lee et al. (2018) established for a limited number of shade types in London, Ontario, Canada. They found building shade to be most effective followed by trees and umbrellas. In contrast, Du et al. (2020) observed an average T_{MRT} reduction of 28.1°C for trees and 28.8°C for buildings in Harbin, China, but they conducted observations under a cluster of tall elm trees with little direct shortwave radiation penetrating the canopies. Other studies have shown that tree spacing significantly impacts ΔT_{MRT} with clustered trees providing more cooling benefits than single trees (Park et al. 2019; Lee et al. 2020). In a Phoenix, Arizona park, Colter et al. (2019) found 15.0°C to 23.5°C higher T_{MRT} in the sun than under single trees. They showed that desert native *Parkinsonia* and *Prosopis* trees did not reduce T_{MRT} as effectively as non-native *Fraxinus*, *Pinus*,

298 and *Ulmus*, mainly due to reduced LAD and increased SVF under the canopy. Several studies
299 observed elevated T_{MRT} under shade structures and trees after sunset compared to previously sun-
300 exposed locations, showing that non-retractable shade traps emitted longwave radiation at low
301 windspeeds (Shashua-Bar et al. 2011; Middel and Krayenhoff 2019). Nighttime heat retention
302 under shade structures and longwave radiation trapping in urban canyons create a tradeoff
303 between daytime and nighttime heat mitigation that should be investigated further.
304 Middel et al. (2016) did not find a difference in subjective thermal sensation votes under
305 trees and photovoltaic canopy shade, indicating that the shade performance variation sensed by
306 human-biometeorological instruments does not necessarily lead to perceived thermal comfort
307 differences. More research is needed to translate ΔT_{MRT} for each shade type into thermal comfort
308 perceptions using field surveys and measurements. To comprehensively analyze the impact of
309 each shade type on an individual's outdoor thermal comfort, humidity and wind must be
310 included in the analysis as well as physical, psychological, physiological, and behavioral factors.
311 Our study has several limitations. First, the instrumental setup has the inherent constraint
312 that the net radiometers are spaced 90–150 cm apart to minimize the impact of the cart on the
313 sensor readings. When positioning *MaRTy* at a shaded location we ensured that the up/down
314 sensors were centered under the shade, but the lateral sensors were outside the shade perimeter in
315 some cases, which slightly increased T_{MRT}. Although we aimed to choose locations with
316 homogeneous ground surfaces, the downwards facing pyrgeometer (150° field of view) captured
317 other surface type patches in the periphery as well as the cart (view factor of 0.12, see Figure
318 A.15). Additional T_s observations with an infrared thermometer assured that the *MaRTy* observed
319 L_{down} and T_s were not significantly impacted by the large field of view. *MaRTy*'s mobility
320 facilitates transects and provides the ability to observe several locations within a short period, but

Accepted for publication in *Bulletin of the American Meteorological Society.* DOI 10.1175/BAMS-D-20-0193.1.

it also introduces measurement errors for slower sensors. The air temperature probe used in this experiment has a time constant of 22 s (63% step change). Although we removed observations that were affected by this sensor lag, the probe did not have time to fully reach equilibrium during the 45–60 s stop.

Second, we did not systematically analyze the impact of shade size parameters on shade performance. For example, the horizontal extent and height of a shade structure influences shade area coverage. A shade structure with large horizontal extent has a shade performance curve that is stretched towards the tunnel reference curve in the morning and afternoon, while smaller structures such as bus shelters have a u-shaped curve due to sun-exposure in the morning and afternoon. The proximity of the structure to a person's body also impacts T_{MRT} and the shape of the performance curve. Shade types that are close to a person's body dampen the shade curve and slightly increase T_{MRT}. For example, Kántor et al. (2018) found that low-hanging shade sails are less effective in reducing T_{MRT} than high-hanging shade sails and trees.

Third, this study did not systematically investigate the effect of tree traits on shade performance. While we distinguished between tree species and sampled mature trees only, we did not consider the shade factor, transmissivity, leaf area index (LAI), size, and crown shape (pruning practices) of trees. Those parameters impact the amount of radiation that is attenuated and may be more important T_{MRT} regulators than species (McPherson et al. 2018; Konarska et al. 2014). Larger, denser trees in more temperate climates will push the shade performance curve towards the tunnel reference curve, while highly transmissive trees will move the curve towards the x-axis and increase T_{MRT} under the canopy.

Fourth, we prioritized shade type variety over individual shade type sample size, especially with respect to trees. This study focused on the shade efficacy of a diverse sample of

engineered/lightweight shade, shade from urban form, and natural shade towards building a comprehensive shade performance database. Thermal metrics for individual tree species as detailed in the supplemental materials are not generalizable and should be used with caution as sample sizes are small.

Fifth, this study focused on clear sunny days; shade performance will be different under cloudy conditions when direct shortwave radiation is reduced, and longwave radiation becomes the main driver of T_{MRT} (Lee et al. 2018). For overcast skies, the shade performance curves will be close to the x-axis. Performance will also change seasonally with varying solar elevation angle, which may impact shade type ranking and will alter the characteristic shade curves. For example, lower sun angles can increase shade in east-west oriented urban canyons from buildings to the south but decrease shade at bus stops.

Finally, we did not consider mutual shading or multi-layered shade. Coutts et al. (2016) studied street trees in urban canyons in Melbourne, Australia and observed that tall buildings masked the cooling impact of trees. More complex scenarios that include irregular street patterns, different tree layouts, and mutual shading of various urban features should be analyzed systematically.

Isolating shade types from their urban context allowed us to define characteristic curves that conceptualize the shade performance under clear, hot outdoor conditions. While tailored to the Southwest U.S., the curves are applicable to other geographic locations and seasons if adjusted for different solar angles. Cities can use the curves in a multi-criteria decision-making process to find viable shade alternatives in spaces that face urban infrastructure challenges. Once a location has been identified as shade priority, cities should consider the desired timing of shade

366 depending on space use and then, based on infrastructure constraints, choose a shade type with
367 the desired shade outcome (optimized timing and cooling magnitude).

368 **5. Summary and Conclusions**

369 Shade significantly reduces the heat load on the human body and decreases thermal stress on hot
370 sunny days. Understanding the performance of various shade types is critical to support effective
371 deployment of shade in places that face urban infrastructure challenges. The heat mitigation
372 services provided by shade must be understood in their urban context (e.g., underlying surface
373 materials, surrounding urban form) and function of space (e.g., right-of-way, playground, bus
374 stop) to find the best shade strategy for a given location. This study assessed the efficacy of
375 natural and engineered shade in Tempe, Arizona through human-biometeorological field
376 observations that revealed 50 grades of shade among 1988 valid samples at 159 unique locations.
377 During the day, at solar noon, and peak T_a, shade from urban form reduced T_s and T_{MRT} most
378 effectively, followed by trees and lightweight structures. After sunset, T_{MRT} and T_s remained
379 slightly elevated under the shade.

380 We developed shade performance curves that show diurnal ΔT_{MRT} for each isolated shade
381 type under clear, hot outdoor conditions. The curves illustrate the characteristic timing and
382 magnitude of ΔT_{MRT} and will assist the City of Tempe and other municipalities in making
383 evidence-based decisions on effective shade deployment. This study expands the "right tree,
384 right place" paradigm to "right shade, right place" by including viable non-natural shade
385 alternatives into urban design guidelines while acknowledging the co-benefits of trees. This
386 "right shade, right place" approach provides quantitative support for other complementary
387 research examining shade pattern scenarios for future tree planting interventions on pedestrian

388 corridors (Langenheim et al., 2020) including in-situ derived evidence for improving ENVI-met
389 modeling scenarios (Morakinyo et al. 2020; Crank et al. 2020).

390 Besides supporting active shade management, the performance curves also make a
391 theoretical contribution to the field of urban climate, as they constitute a crucial step towards
392 formalizing Micro-Climate Zones (MCZs). Similar to Local Climate Zones (LCZs) that
393 characterize neighborhood-scale temperature differences due to urban form, function, and
394 materials (Stewart and Oke 2012), MCZs can be defined as human-scale (1–10 m^2) zones that
395 exhibit characteristic diurnal thermal profiles (T_a, T_{MRT}, and T_s) driven by the urban form,
396 function, and materials in the immediate surroundings of a person. While LCZs are local in scale
397 and encompass a wide range of T_{MRT} and T_s values per zone, MCZs are nested inside a particular
398 LCZ and are characterized by typical longwave and shortwave radiation signatures that lead to a
399 distinct thermal exposure (i.e., shade performance curves) driven by shade and surrounding
400 surface properties. More empirical data and human-biometeorological observations are needed to
401 solidify this concept. Ultimately, the fine scale of MCZs would prompt designers of the urban
402 environment (architects, landscape architects, and urban designers) to assess the thermal
403 performance of their design from a human-centric perspective during the decision-making
404 process.

REFERENCES

de Abreu-Harbich, L. V., L. C. Labaki, and A. Matzarakis, 2015: Effect of tree planting design and tree species on human thermal comfort in the tropics. *Landsc. Urban Plan.*, **138**, 99–109, https://doi.org/10.1016/j.landurbplan.2015.02.008.

Ali-Toudert, F., and H. Mayer, 2007: Thermal comfort in an east–west oriented street canyon in Freiburg (Germany) under hot summer conditions. *Theor. Appl. Climatol.*, **87**, 223–237, https://doi.org/10.1007/s00704-005-0194-4.

Aminipouri, M., A. J. Knudby, E. S. Krayenhoff, K. Zickfeld, and A. Middel, 2019: Modelling the impact of increased street tree cover on mean radiant temperature across Vancouver's local climate zones. *Urban For. Urban Green.*, **39**, 9–17, https://doi.org/10.1016/j.ufug.2019.01.016.

Armson, D., M. A. Rahman, and A. R. Ennos, 2013: A comparison of the shading effectiveness of five different street tree species in Manchester, UK. *Arboric. Urban For.*, **39**, 157–164.

Bowler, D. E., L. Buyung-Ali, T. M. Knight, and A. S. Pullin, 2010: Urban greening to cool towns and cities: A systematic review of the empirical evidence. *Landsc. Urban Plan.*, **97**, 147–155, https://doi.org/10.1016/j.landurbplan.2010.05.006.

Cheung, P. K., and C. Y. Jim, 2018: Comparing the cooling effects of a tree and a concrete shelter using PET and UTCI. *Build. Environ.*, **130**, 49–61, https://doi.org/10.1016/j.buildenv.2017.12.013.

City of Sydney, 2013: *Urban Forest Strategy*. https://www.cityofsydney.nsw.gov.au/-/media/corporate/files/2020-07-migrated/files_u/urban-forest-strategy-adopted-feb-2013.pdf?download=true.

City of Tempe, 2017: *City of Tempe Urban Forestry Master Plan*. https://www.tempe.gov/home/showdocument?id=54581.

Colter, K. R., A. C. Middel, and C. A. Martin, 2019: Effects of natural and artificial shade on human thermal comfort in residential neighborhood parks of Phoenix, Arizona, USA. *Urban For. Urban Green.*, **44**, 126429, https://doi.org/10.1016/j.ufug.2019.126429.

Coutts, A. M., E. C. White, N. J. Tapper, J. Beringer, and S. J. Livesley, 2016: Temperature and human thermal comfort effects of street trees across three contrasting street canyon environments. *Theor. Appl. Climatol.*, **124**, 55–68, https://doi.org/10.1007/s00704-015-1409-y.

Crank, P. J., A. Middel, M. Wagner, D. Hoots, M. Smith, and A. Brazel, 2020: Validation of seasonal mean radiant temperature simulations in hot arid urban climates. *Sci. Total Environ.*, **749**, 141392, https://doi.org/10.1016/j.scitotenv.2020.141392.

Crewe, K., A. Brazel, and A. Middel, 2016: Desert New Urbanism: testing for comfort in downtown Tempe, Arizona. *J. Urban Des.*, **21**, 746–763, https://doi.org/10.1080/13574809.2016.1187558.

Downs, N. J., L. Baldwin, A. V. Parisi, H. J. Butler, J. Vanos, M. Beckman, and S. Harrison, 2019: Comparing the annualised dynamic shade characteristics of twenty-one tree canopies across twenty-six municipalities in a high ambient UV climate, Queensland - Australia. *Appl. Geogr.*, **108**, 74–82, https://doi.org/10.1016/j.apgeog.2019.05.006.

Du, J., L. Liu, X. Chen, and J. Liu, 2020: Field Assessment of Neighboring Building and Tree Shading Effects on the 3D Radiant Environment and Human Thermal Comfort in Summer within Urban Settlements in Northeast China. *Adv. Meteorol.*, **2020**, https://doi.org/10.1155/2020/8843676.

Emmanuel, R., H. Rosenlund, and E. Johansson, 2007: Urban shading - A design option for the tropics? A study in Colombo, Sri Lanka. *Int. J. Climatol.*, **27**, 1995–2004, https://doi.org/10.1002/joc.1609.

Garcia-Nevado, E., B. Beckers, and H. Coch, 2020: Assessing the Cooling Effect of Urban Textile Shading Devices Through Time-Lapse Thermography. *Sustain. Cities Soc.*, **63**, 102458, https://doi.org/10.1016/j.scs.2020.102458.

Golden, J. S., J. Carlson, K. E. Kaloush, and P. Phelan, 2007: A comparative study of the thermal and radiative impacts of photovoltaic canopies on pavement surface temperatures. *Sol. Energy*, **81**, 872–883, https://doi.org/10.1016/j.solener.2006.11.007.

Gregory McPherson, E., 1992: Accounting for benefits and costs of urban greenspace. *Landsc. Urban Plan.*, **22**, 41–51, https://doi.org/10.1016/0169-2046(92)90006-L.

Häb, K., B. L. Ruddell, and A. Middel, 2015: Sensor lag correction for mobile urban microclimate measurements. *Urban Clim.*, **14**, 622–635, https://doi.org/10.1016/j.uclim.2015.10.003.

Höppe, P., 1992: A new procedure to determine the mean radiant temperature outdoors. *Wetter und Leb.*,.

Johansson, E., and R. Emmanuel, 2006: The influence of urban design on outdoor thermal comfort in the hot, humid city of Colombo, Sri Lanka. *Int. J. Biometeorol.*, **51**, 119–133, https://doi.org/10.1007/s00484-006-0047-6.

Kántor, N., and J. Unger, 2011: The most problematic variable in the course of human-biometeorological comfort assessment - The mean radiant temperature. *Cent. Eur. J. Geosci.*, **3**, 90–100, https://doi.org/10.2478/s13533-011-0010-x.

——, A. Kovács, and Á. Takács, 2016: Small-scale human-biometeorological impacts of shading by a large tree. *Open Geosci.*, **8**, 231–245, https://doi.org/10.1515/geo-2016-0021.

Klemm, W., B. G. Heusinkveld, S. Lenzholzer, and B. van Hove, 2015: Street greenery and its physical and psychological impact on thermal comfort. *Landsc. Urban Plan.*, **138**, 87–98, https://doi.org/10.1016/j.landurbplan.2015.02.009.

Konarska, J., F. Lindberg, A. Larsson, S. Thorsson, and B. Holmer, 2014: Transmissivity of solar radiation through crowns of single urban trees-application for outdoor thermal comfort modelling. *Theor. Appl. Climatol.*, **117**, 363–376, https://doi.org/10.1007/s00704-013-1000-

3.

Langenheim, N., M. White, N. Tapper, S. J. Livesley, and D. Ramirez-Lovering, 2020: Right tree, right place, right time: A visual-functional design approach to select and place trees for optimal shade benefit to commuting pedestrians. *Sustain. Cities Soc.*, **52**, https://doi.org/10.1016/j.scs.2019.101816.

Lee, H., H. Mayer, and W. Kuttler, 2020: Impact of the spacing between tree crowns on the mitigation of daytime heat stress for pedestrians inside E-W urban street canyons under Central European conditions. *Urban For. Urban Green.*, https://doi.org/10.1016/j.ufug.2019.126558.

Lee, I., J. A. Voogt, and T. J. Gillespie, 2018: Analysis and comparison of shading strategies to increase human thermal comfort in urban areas. *Atmosphere (Basel).*, **9**, https://doi.org/10.3390/atmos9030091.

Lindberg, F., and C. S. B. Grimmond, 2011: The influence of vegetation and building morphology on shadow patterns and mean radiant temperatures in urban areas: Model development and evaluation. *Theor. Appl. Climatol.*, **105**, 311–323, https://doi.org/10.1007/s00704-010-0382-8.

McPherson, E. G., Q. Xiao, N. S. van Doorn, N. Johnson, S. Albers, and P. J. Peper, 2018: Shade factors for 149 taxa of in-leaf urban trees in the USA. *Urban For. Urban Green.*, **31**, 204–211, https://doi.org/10.1016/j.ufug.2018.03.001.

Meehl, G. A., and C. Tebaldi, 2004: More intense, more frequent, and longer lasting heat waves in the 21st century. *Science (80-.).*, https://doi.org/10.1126/science.1098704.

Middel, A., and E. S. Krayenhoff, 2019: Micrometeorological determinants of pedestrian thermal exposure during record-breaking heat in Tempe, Arizona: Introducing the MaRTy observational platform. *Sci. Total Environ.*, **687**, 137–151, https://doi.org/10.1016/j.scitotenv.2019.06.085.

——, A. J. Brazel, S. Kaplana, and S. W. Myint, 2012: Daytime cooling efficiency and diurnal energy balance in Phoenix, Arizona, USA. *Clim. Res.*, **54**, 21–34, https://doi.org/10.3354/cr01103.

——, K. Häb, A. J. Brazel, C. A. Martin, and S. Guhathakurta, 2014: Impact of urban form and design on mid-afternoon microclimate in Phoenix Local Climate Zones. *Landsc. Urban Plan.*, **122**, 16–28, https://doi.org/10.1016/j.landurbplan.2013.11.004.

——, N. Selover, B. Hagen, and N. Chhetri, 2016: Impact of shade on outdoor thermal comfort—a seasonal field study in Tempe, Arizona. *Int. J. Biometeorol.*, **60**, 1849–1861, https://doi.org/10.1007/s00484-016-1172-5.

——, J. Lukasczyk, S. Zakrzewski, M. Arnold, and R. Maciejewski, 2019: Urban form and composition of street canyons: A human-centric big data and deep learning approach. *Landsc. Urban Plan.*, **183**, 122–132, https://doi.org/10.1016/j.landurbplan.2018.12.001.

——, V. K. Turner, F. A. Schneider, Y. Zhang, and M. Stiller, 2020: Solar reflective pavements-

A policy panacea to heat mitigation? *Environ. Res. Lett.*, **15**, https://doi.org/10.1088/1748-9326/ab87d4.

Morakinyo, T. E., W. Ouyang, K. K. L. Lau, C. Ren, and E. Ng, 2020: Right tree, right place (urban canyon): Tree species selection approach for optimum urban heat mitigation - development and evaluation. *Sci. Total Environ.*, **719**, https://doi.org/10.1016/j.scitotenv.2020.137461.

Norton, B. A., A. M. Coutts, S. J. Livesley, R. J. Harris, A. M. Hunter, and N. S. G. Williams, 2015: Planning for cooler cities: A framework to prioritise green infrastructure to mitigate high temperatures in urban landscapes. *Landsc. Urban Plan.*, **134**, 127–138, https://doi.org/10.1016/j.landurbplan.2014.10.018.

Parisi, A. V., A. Amar, N. J. Downs, D. P. Igoe, S. L. Harrison, and J. Turner, 2019: Development of a model for calculating the solar ultraviolet protection factor of small to medium sized built shade structures. *Build. Environ.*, **147**, 415–421, https://doi.org/10.1016/j.buildenv.2018.10.010.

Park, C. Y., D. K. Lee, E. S. Krayenhoff, H. K. Heo, J. H. Hyun, K. Oh, and T. Y. Park, 2019: Variations in pedestrian mean radiant temperature based on the spacing and size of street trees. *Sustain. Cities Soc.*, **48**, https://doi.org/10.1016/j.scs.2019.101521.

Pataki, D. E., and Coauthors, 2011: Coupling biogeochemical cycles in urban environments: ecosystem services, green solutions, and misconceptions. *Front. Ecol. Environ.*, **9**, 27–36, https://doi.org/10.1890/090220.

Pearlmutter, D., A. Bitan, and P. Berliner, 1999: Microclimatic analysis of "compact" urban canyons in an arid zone. *Atmospheric Environment*, Vol. 33 of, 4143–4150.

Roman, L. A., and Coauthors, 2020: Beyond 'trees are good': Disservices, management costs, and tradeoffs in urban forestry. *Ambio*, https://doi.org/10.1007/s13280-020-01396-8.

Salmond, J. A., and Coauthors, 2016: Health and climate related ecosystem services provided by street trees in the urban environment. *Environ. Heal. A Glob. Access Sci. Source*, **15**, https://doi.org/10.1186/s12940-016-0103-6.

Shashua-Bar, L., D. Pearlmutter, and E. Erell, 2011: The influence of trees and grass on outdoor thermal comfort in a hot-arid environment. *Int. J. Climatol.*, **31**, 1498–1506, https://doi.org/10.1002/joc.2177.

Speak, A., L. Montagnani, C. Wellstein, and S. Zerbe, 2020: The influence of tree traits on urban ground surface shade cooling. *Landsc. Urban Plan.*, **197**, 103748, https://doi.org/10.1016/j.landurbplan.2020.103748.

Stewart, I. D., and T. R. Oke, 2012: Local climate zones for urban temperature studies. *Bull. Am. Meteorol. Soc.*, **93**, 1879–1900, https://doi.org/10.1175/BAMS-D-11-00019.1.

The City of Austin, 2013: *Austin's Urban Forest Plan: A Master Plan for Public Property*. https://www.austintexas.gov/sites/default/files/files/Parks/Forestry/AUFP_Final_DRAFT_01-07-14_No_Appendices.pdf.

VDI, 1998: *VDI 3787 Part I: environmental meteorology, methods for the human-biometeorological evaluation of climate and air quality for the urban and regional planning at regional level. Part I: climate.* 29 pp.

Table 1: *MaRTy* instrument platform specifics: sensor ranges, accuracies, and heights above ground.

	Sensor	Variable(s)	Range	Accuracy	Sensor Time Constant/Response Time	Height
A	EE181 (Pt1000 Class A, HC101)	Temperature	-40–60°C	±0.2°C	[63% step change (1 m s^{-1} air flow at sensor)] ≤22 s	1.5 m
		Relative Humidity	0–100%	-15–40°C: ≤90% RH ± (1.3 + 0.003 • RH reading) % RH -15–40°C: >90% RH ± 2.3% RH -25–60°C: ± (1.4 + 0.01 • RH reading) % RH -40–60°C: ± (1.5 + 0.015 • RH reading) % RH	[63% of a 35 to 80% RH step change (1 m s^{-1} air flow at sensor)] ≤22 s	1.5 m
B	Gill 2D WindSonic	Wind Speed	0–60 m s^{-1} (116 knots)	±2% @12 m s^{-1}	0.25 seconds	1.7 m
		Wind Direction	0–360°	±2° @12 m s^{-1}		
C	GPS16X Garmin GPS	Latitude/Longitude	Temperature: -30–80 °C operational	Position: Less than 15 m, 95% typical (100 m with selective availability on)	1 s (all data known)	1.5 m
				Velocity: 0.1 knot RMS steady state		
D	3 NR01 Hukseflux 4-Component Net Radiometers (oriented u/down, left/right, front/back)	Shortwave radiation	–2000 W m^{-2}; spectral range 305–2800 nm (50% transmission points)	± 10% for 12 hour totals, day and night	[for 95% response] 18 s	1.1–1.3 m
		Longwave radiation	–1000 W m^{-2}; spectral range 4500–50000 nm (50% transmission points)			

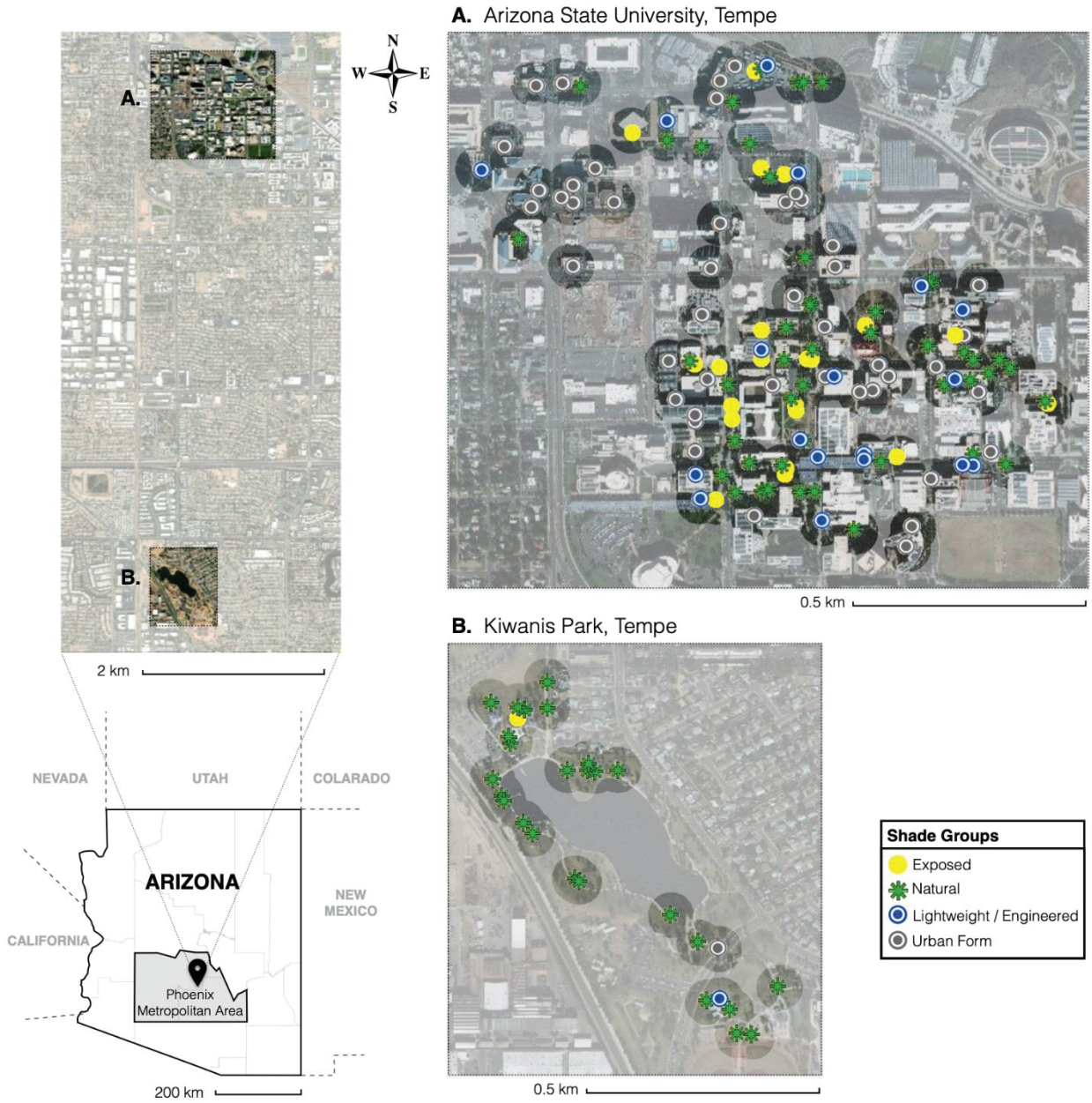

Figure 1: Aerial view of study areas in the City of Tempe: A. Downtown Tempe including the Mill Avenue District (to the north-west) and Arizona State University's Tempe Campus (to the south-east); B. Kiwanis Park.

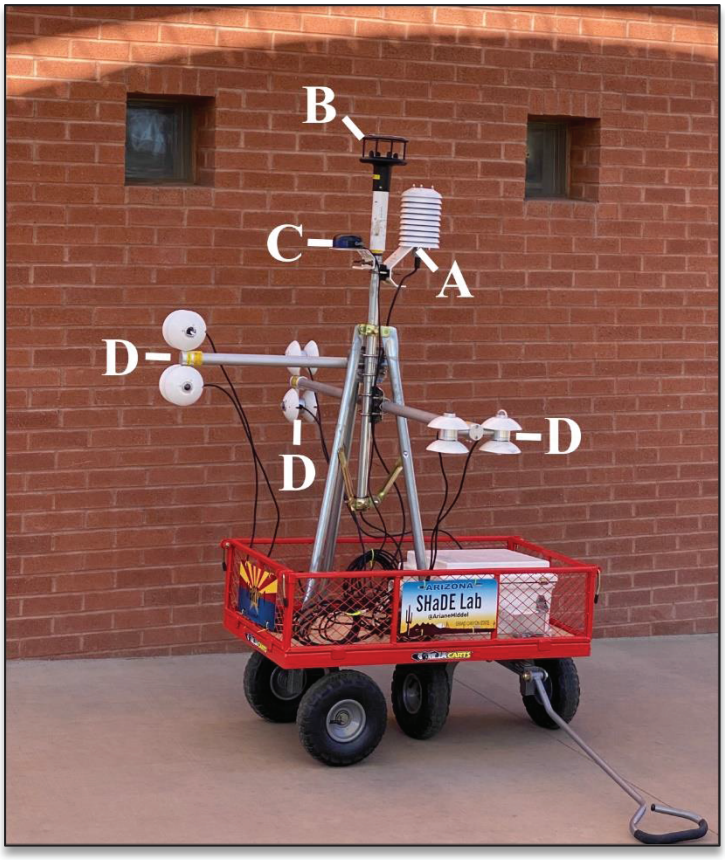

Figure 2: The mobile human-biometeorological instrument platform *MaRTy* (Middel and Krayenhoff 2019; Middel et al. 2020). A) EE181 temperature/humidity probe, B) Gill 2D WindSonic horizontal wind speed/direction sensor, C) GPS16X Garmin GPS sensor, D) three NR01 Hukseflux 4-Component Net Radiometers to measure shortwave and longwave radiation in 6 directions (up/down, left/right, back/front). Sensor heights and specifications listed in Table 1.

Accepted for publication in *Bulletin of the American Meteorological Society*. DOI 10.1175/BAMS-D-20-0193.1.

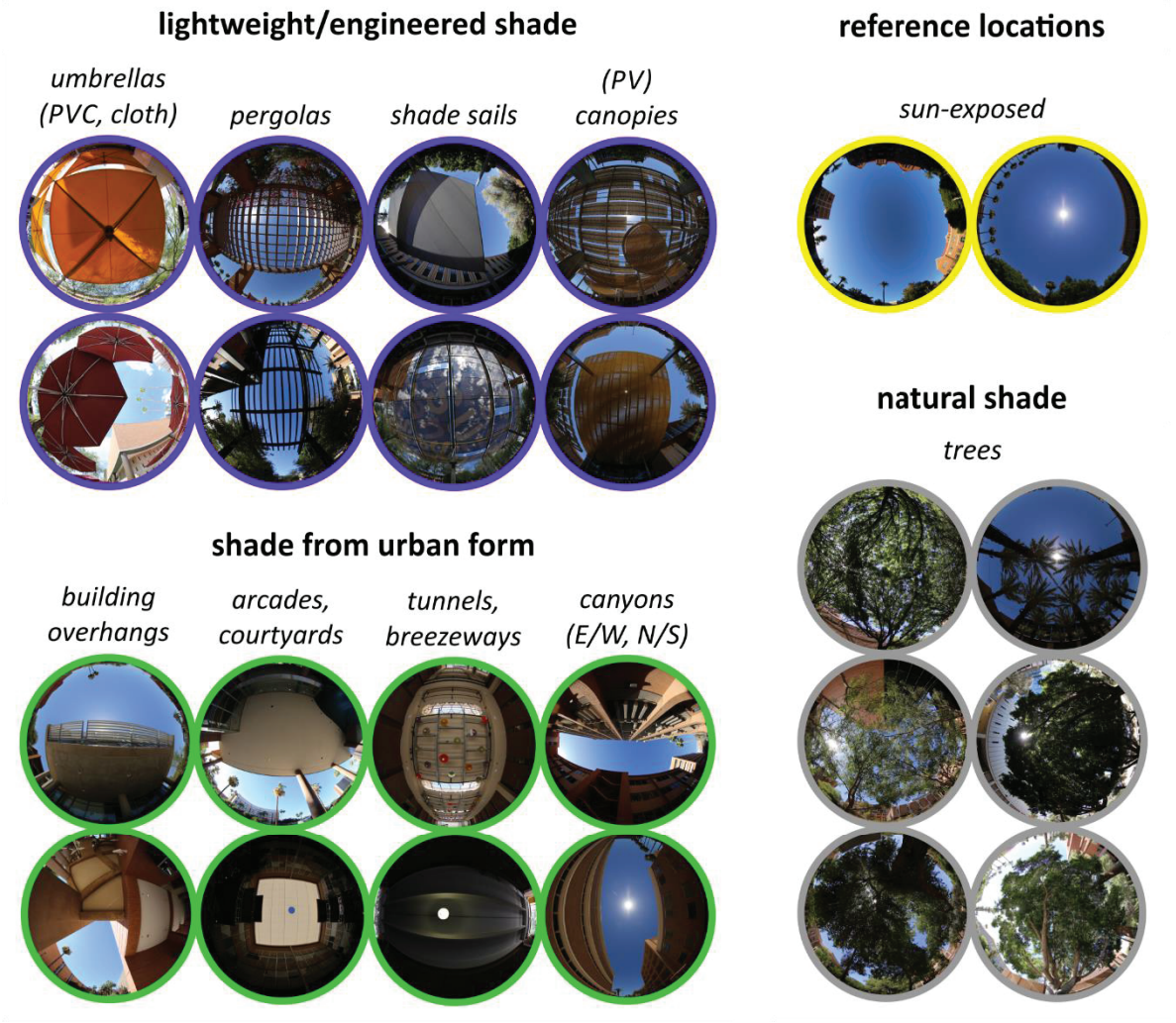

Figure 3: Sample of hemispherical fisheye photos for three shade groups with various shade types and sun-exposed reference locations; photos were taken at 1.1 m height with a Canon EOS 6D and Canon EF 8-15-mm f/4 Fisheye USM Ultra-Wide Zoom lens pointing upwards.

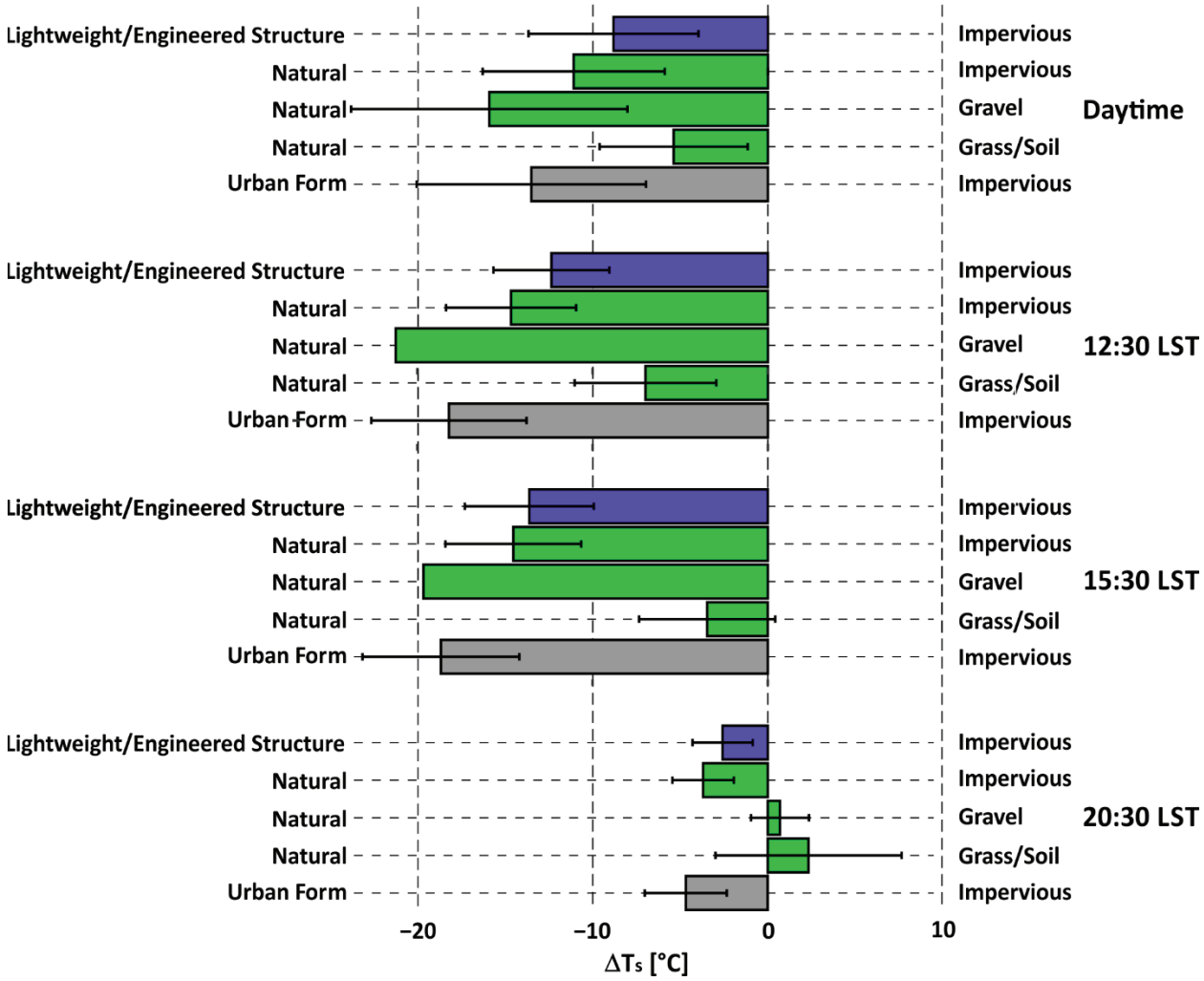

Figure 4: Observed surface temperature reduction (ΔT_s) of impervious surfaces, gravel, and grass/soil by shade group for daytime, 12:30 LST, 15:30 LST, and 20:30 LST. Note that only one gravel location was observed at 12:30 LST and 15:30 LST.

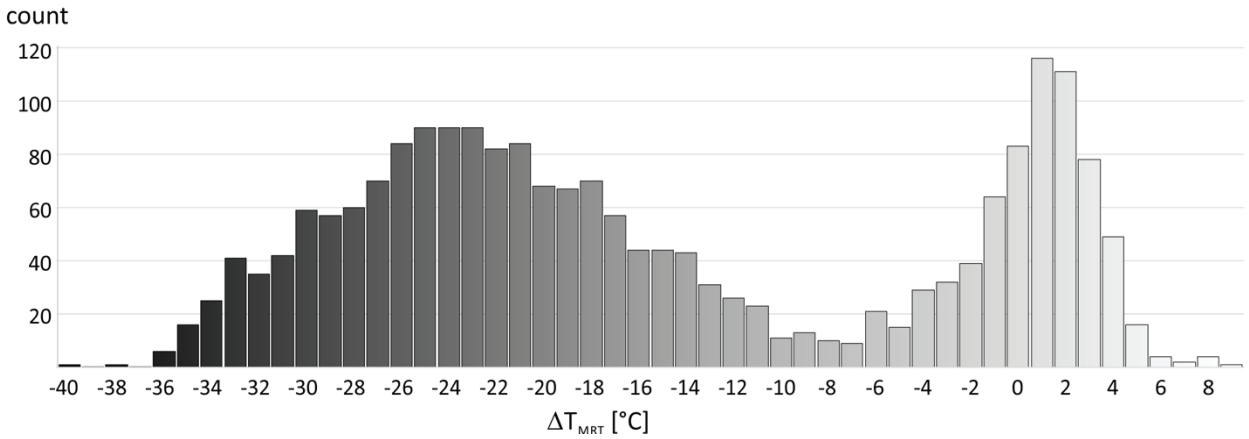

Figure 5: 50 grades of shade: difference in mean radiant temperature (ΔT_{MRT}) between all locations and corresponding sun-exposed reference locations for all times, days, and sites (n = 1988, 159 sites).

Accepted for publication in *Bulletin of the American Meteorological Society.* DOI 10.1175/BAMS-D-20-0193.1.

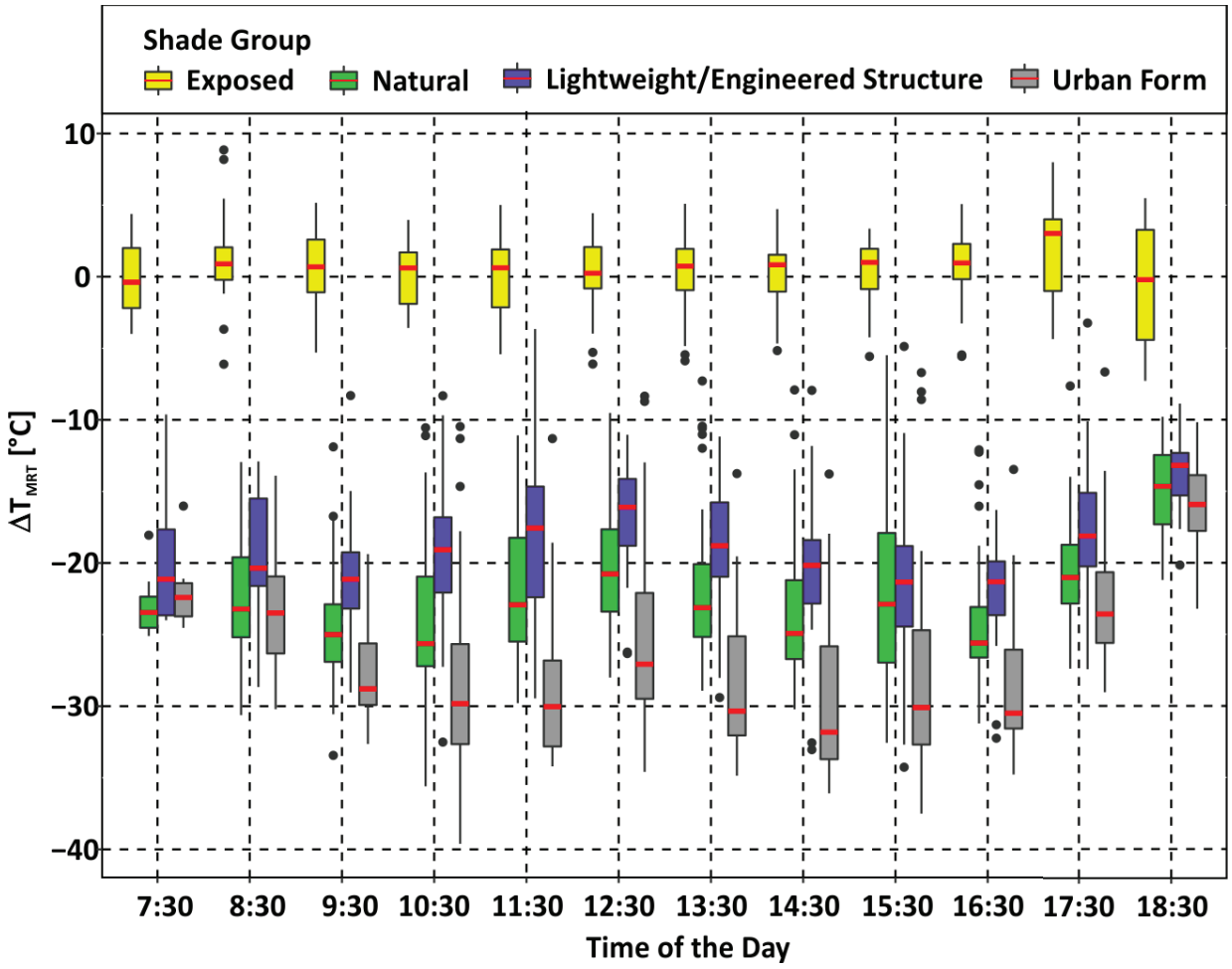

Figure 6: Boxplot of time-detrended hourly mean radiant temperature differences (ΔT_{MRT}) between exposed reference locations (yellow) and locations shaded by trees (green), lightweight/engineered structures (blue), and urban form (grey). The 0 line is based on the mean of all sun-exposed locations.

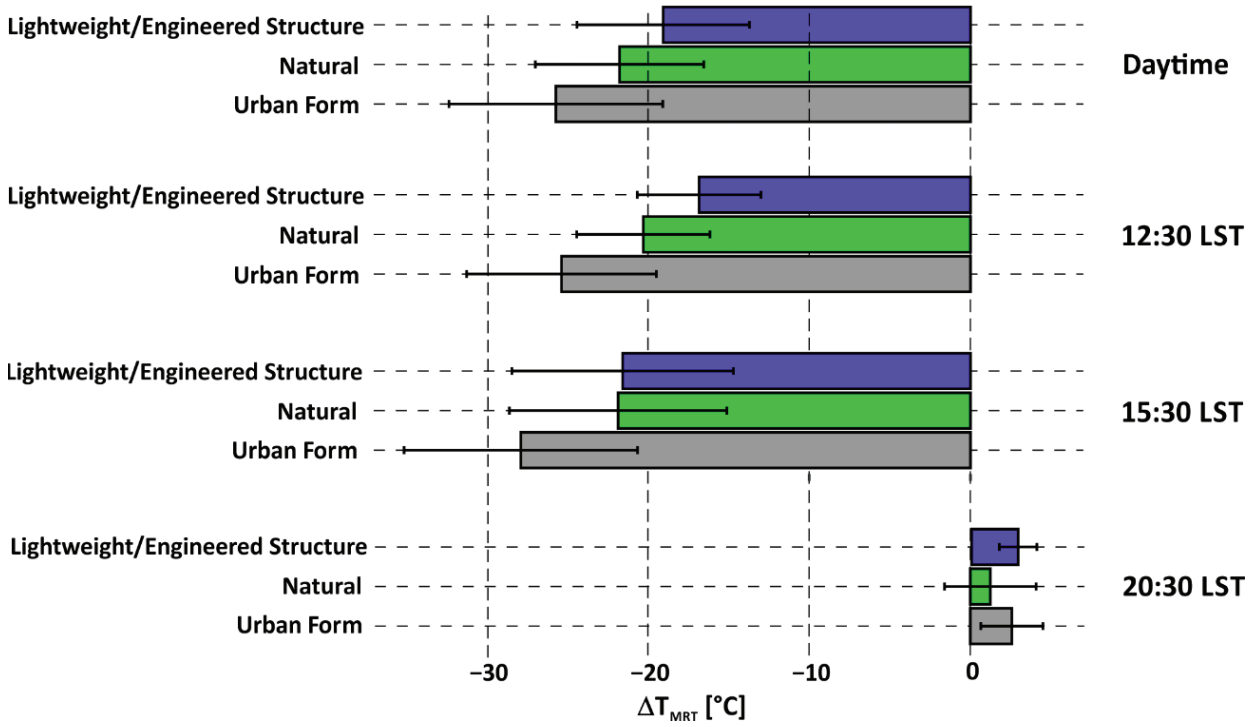

Figure 7: Observed time-detrended mean radiant temperature reduction (ΔT_{MRT}) by shade group for daytime, 12:30 LST, 15:30 LST, and 20:30 LST (after sunset).

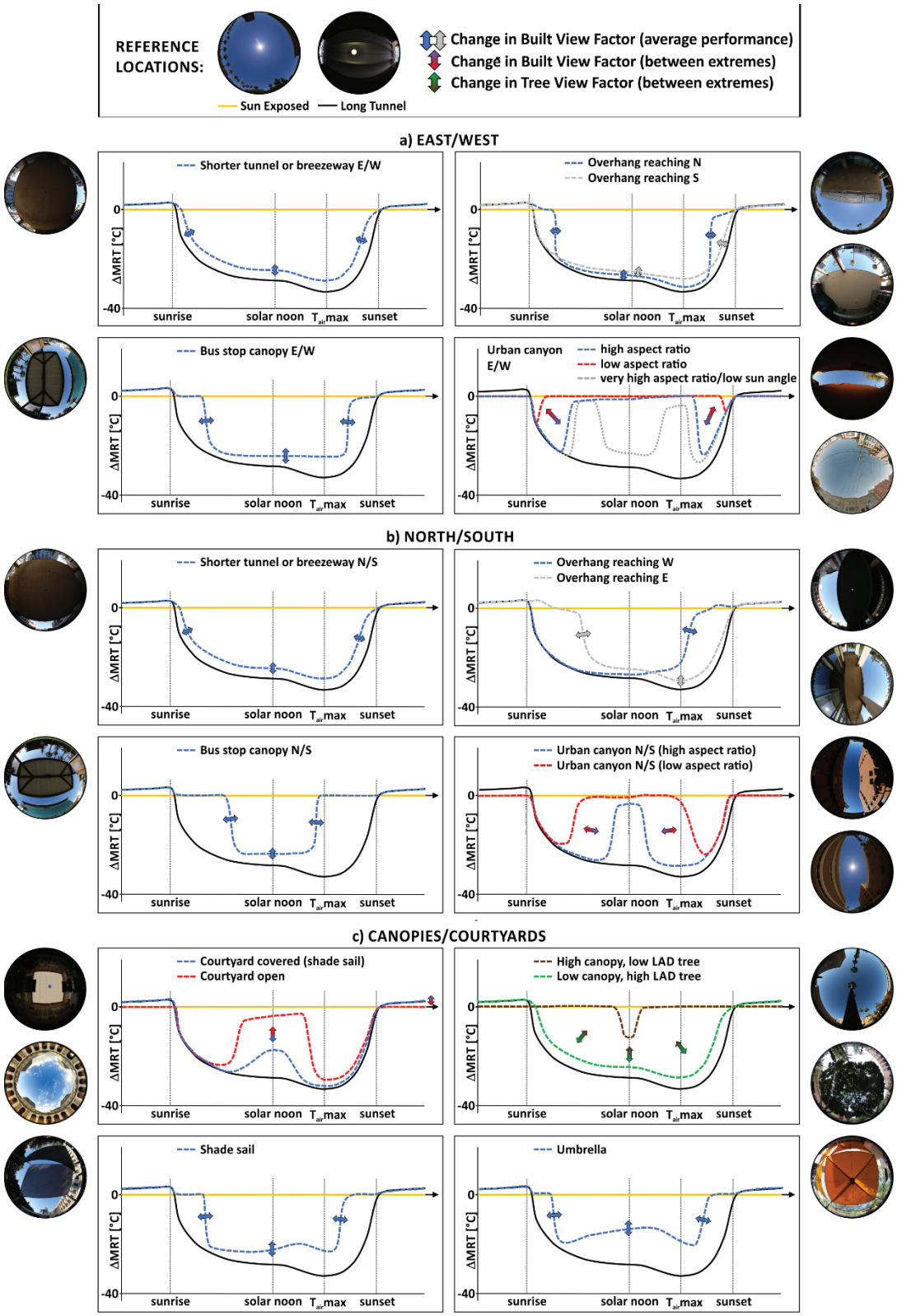

Figure 8: Characteristic shade performance curves for all shade types under investigation organized by orientation: a) east/west, b) north-south, and c) canopies/courtyards (orientation

Accepted for publication in *Bulletin of the American Meteorological Society*. DOI 10.1175/BAMS-D-20-0193.1.

independent). Empirically based curves display the evolution of ΔT_{MRT} under idealized shade types (no surrounding urban form, fisheye photos are for illustration only) assuming a latitude of 33° and a sun path for mid-July. Curves refer to a person standing in the center of the fisheye photo.